Cross-Polarization from Quadrupolar Nuclei to Silicon Using Low-Radio-Frequency Amplitudes during Magic-Angle Spinning

Susan M. De Paul,[†] Matthias Ernst,[†,§] Jay S. Shore,[†,⊥] Jonathan F. Stebbins,[‡] and Alexander Pines*,[†]

Materials Sciences Division, E. O. Lawrence Berkeley National Laboratory, 1 Cyclotron Road, Berkeley, California 94720, Department of Chemistry, University of California, Berkeley, California 94720, and Department of Geology, Stanford University, Stanford, California 94305

Received: August 6, 1996; In Final Form: February 6, 1997[⊗]

The dynamics of cross-polarization from the central transition of a quadrupolar nucleus (^{27}Al or ^{23}Na) to a spin-$^1/_2$ nucleus (^{29}Si) during magic-angle spinning and using low-radio-frequency field strengths are analyzed for the mineral low albite. Under these conditions additional complications in the spin-lock behavior of the quadrupolar nucleus and in the cross-polarization process were found experimentally and are examined in detail. A step-by-step procedure for optimizing cross-polarization from the central transition of a quadrupolar nucleus to a spin-$^1/_2$ nucleus is described. Significant enhancement of ^{29}Si NMR sensitivity and several applications are demonstrated.

1. Introduction

Silicon is an important component of many inorganic materials including zeolites, glasses, minerals, and gels. Since these materials often have limited long-range order, solid-state ^{29}Si NMR has proven to be particularly useful in eliciting information about their structure.[1,2] However, the low natural abundance of ^{29}Si (4.7%) combined with its relatively low gyromagnetic ratio makes ^{29}Si NMR inherently insensitive. Furthermore, significant improvement of the signal-to-noise ratio by signal averaging is usually time-consuming due to the typically long T_1 relaxation times of ^{29}Si (frequently on the order of minutes). Consequently, two-dimensional experiments are often impractical, unless isotopic enrichment or cross-polarization (CP)[3] is used. Although cross-polarization from protons to silicon can greatly enhance ^{29}Si NMR intensities, not all silicates of interest contain protons. Many silicates do contain quadrupolar nuclei such as ^{27}Al or ^{23}Na, which are 100% naturally abundant and can be used as magnetization sources during cross-polarization.

Cross-polarization is a process by which magnetization is transferred from one spin species to another. Each spin species is subjected to radio-frequency (rf) irradiation in the form of a spin-lock field; the amplitudes of these spin-lock fields are adjusted to permit energy-conserving magnetization transfer between the two types of spins. Cross-polarization can lead to an enhancement of the relative sensitivity of a nucleus in two ways: (1) by transferring magnetization from a nucleus with a higher gyromagnetic ratio (utilizing the different Boltzmann distribution) or (2) by increasing the repetition rate of the experiment (utilizing differences in the relaxation rates). Although cross-polarization between two spin-$^1/_2$ nuclei during magic-angle spinning (MAS) is routine,[4,5] cross-polarization involving quadrupolar nuclei such as aluminum or sodium is more complicated because the efficiency of a spin lock on a quadrupolar nucleus depends on the relative magnitudes of the rotor spinning speed, the quadrupolar coupling constant, and the applied spin-lock field strength.[6,7] Cross-polarization from quadrupolar nuclei during MAS has only recently been utilized,[8−12] and most of these studies have focused on assigning peaks or determining connectivities rather than on enhancing sensitivity.

TABLE 1: Silicon Sites in Low Albite ($NaAlSi_3O_8$)

isotropic shift[a] (ppm)	crystallographic T-site	no. of Al nearest neighbors	distance to Al nearest neighbor(s)[b] (Å)	distance to nearest Na[b] (Å)
−91.8	T2m	2	3.019 3.080	3.291
−96.1	T2O	1	3.132	3.494
−103.9	T1m	1	3.156	3.394

[a] Chemical shift values were referenced to an external TMS standard and are within 1 ppm of literature values.[13,15−18] [b] Distances determined using neutron diffraction data from Harlow et al.[14]

The feldspar low albite ($NaAlSi_3O_8$) was chosen as a model compound for ^{27}Al-to-^{29}Si and ^{23}Na-to-^{29}Si cross-polarization experiments for several reasons. In many ways low albite is a typical inorganic aluminosilicate, composed of a framework of connected AlO_4 and SiO_4 tetrahedra and nonframework, charge-balancing counterions (in this case Na^+).[13] The analysis of cross-polarization from the quadrupolar nuclei in low albite is simplified by the presence of only one crystallographic ^{27}Al site and one ^{23}Na site. Furthermore, low albite is highly ordered with the silicon occupying three distinct crystallographic T-sites in equal amounts.[14] Two of these sites are coordinated via bridging oxygens to one aluminum atom and three silicon atoms and are commonly denoted as Q^4(1Al) sites. The superscript 4 indicates that all four oxygens are bridging, and the integer 1 indicates the presence of a single aluminum "nearest neighbor". The third silicon site is coordinated via bridging oxygen to two aluminum and two silicon atoms and is denoted as a Q^4(2Al) site. Assignment of these silicon sites to three distinct and narrow ^{29}Si MAS NMR resonances can be found in the literature.[13,15−18] Table 1 lists these assignments along with the distances between each silicon site and its nearest aluminum and sodium neighbors.

This detailed study was prompted by the technological and geochemical importance of aluminosilicates and sodium sili-

† University of California, Berkeley.
‡ Stanford University.
§ Present address: Laboratory for Physical Chemistry, University of Nijmegen, Toernooiveld, NL-6525 ED Nijmegen, The Netherlands.
⊥ Present address: Department of Chemistry and Biochemistry, South Dakota State University, Brookings, SD 57007.
* To whom correspondence should be addressed.
⊗ Abstract published in *Advance ACS Abstracts,* April 1, 1997.

S1089-5647(96)02371-1 CCC: $14.00

cates, the potential benefits of ^{27}Al-to-^{29}Si and ^{23}Na-to-^{29}Si cross-polarization for sensitivity enhancement, and the difficulties in interpreting the intensities of signals obtained by cross-polarization from quadrupolar nuclei.

The material in this paper is presented as follows. Section 2 compares experimental results with numerical simulations of the spin-locking behavior of half-integer quadrupolar nuclei under low-rf field strengths and MAS. In section 3 the dynamics of cross-polarization from quadrupolar nuclei to spin-$^1/_2$ nuclei are analyzed. Section 4 discusses the signal-to-noise enhancement per unit time achievable by cross-polarization from half-integer quadrupolar nuclei, the advantages and limitations of the technique, and some potential applications.

2. Spin Locking of Half-Integer Quadrupolar Nuclei

Since cross-polarization can only occur if both spins can be spin locked long enough for magnetization to be transferred, it is necessary to determine the conditions under which efficient spin locking is possible. Both spin-$^1/_2$ and quadrupolar nuclei undergo relaxation during a spin lock, characterized by one or several rotating-frame relaxation time constants, $T_{1\rho}$. However, the behavior of the central transition of a half-integer quadrupolar nucleus during a spin lock is also influenced by the time dependence of the quadrupolar coupling under MAS, which can dramatically reduce the spin-locking efficiency for certain combinations of rf field strengths, spinning speeds, and quadrupolar coupling constants. A theoretical treatment of some of these interference effects has been given in the literature[6,7,19,20] and will be summarized here. Throughout this paper the *S* spin refers to the quadrupolar nucleus (^{27}Al or ^{23}Na) and the *I* spin to the spin-$^1/_2$ nucleus (^{29}Si).

When a spin-lock field is applied to a quadrupolar nucleus, the rotating-frame Hamiltonian can be written (in units of angular frequency) as follows

$$\tilde{H} = \omega_{1S} S_x + \Delta\omega S_z + \tilde{H}_Q \tag{1}$$

where ω_{1S} is strength of the rf field used for the spin lock, $\Delta\omega$ is the offset of the irradiation from the Larmor frequency, and $\tilde{H}_Q$ is the rotating-frame quadrupolar Hamiltonian. The quadrupolar Hamiltonian in the rotating frame can be expressed in terms of irreducible spherical tensor operators,[21] and an operator form of static perturbation theory can then be applied.[22] This procedure gives a first-order term

$$\tilde{H}_Q^{(1)} = (\omega_Q/3)\mathbf{R}_{20}^Q \mathbf{T}_{20}^Q \tag{2}$$

where $\mathbf{R}_{20}^Q$ and $\mathbf{T}_{20}^Q$ are spatial and spin tensors, respectively,[21] and ω_Q is the quadrupolar coupling constant

$$\omega_Q = \frac{3e^2qQ}{2S(2S-1)\hbar} = \frac{6\pi}{2S(2S-1)} C_{qcc} \tag{3}$$

The second-order contribution to the quadrupolar Hamiltonian is

$$\tilde{H}_Q^{(2)} = \frac{\hbar\omega_Q^2}{18\omega_L}\{2\mathbf{R}_{21}^Q \mathbf{R}_{2-1}^Q[\mathbf{T}_{21}^Q, \mathbf{T}_{2-1}^Q] + \mathbf{R}_{22}^Q \mathbf{R}_{2-2}^Q[\mathbf{T}_{22}^Q, \mathbf{T}_{2-2}^Q]\} \tag{4}$$

where ω_L is the Larmor frequency.

Because the $\mathbf{R}_{2m}^Q$ terms in eqs 2 and 4 are orientation-dependent, the pattern of energy level spacings for a quadrupolar nucleus under a spin lock differs for different orientations of a crystallite with respect to the static magnetic field. This creates complications when a sample is spun about the magic angle since the spinning process changes the orientations of the crystallites in a powder sample. Considering just the first-order term of the quadrupolar Hamiltonian (eq 2), one can show that the sign of $\tilde{H}_Q^{(1)}$ can change zero, two, or four times per rotor cycle. The resulting time-dependent variation of the energy levels can significantly influence the efficiency of the spin lock. To characterize this behavior, an adiabaticity parameter, α, has been defined[6,7]

$$\alpha = \omega_{1S}^2/\omega_Q\omega_r \tag{5}$$

where ω_r is the spinning speed. While the definition of the adiabaticity parameter can be refined to explicitly include individual crystallite orientations,[19,23] eq 5 is adequate for a qualitative description of the observed experimental behavior. For nuclei in which $\omega_Q \gg \omega_{1S}$, three regimes of spin-locking behavior have been defined based on the rate at which $\tilde{H}_Q^{(1)}$ changes sign. The adiabatic-passage regime ($\alpha \gg 1$) and the sudden-passage regime ($\alpha \ll 1$) permit efficient spin locking by different mechanisms, but in the intermediate regime ($\alpha \approx 1$ theoretically, $\alpha \approx 0.4$ experimentally[6]) spin locking is very inefficient. We will show that even in the sudden-passage regime, efficient spin locks are not always possible.

TABLE 2: Quadrupolar Parameters in Low Albite ($NaAlSi_3O_8$)

nucleus	C_{qcc} (MHz)	η	ref
^{27}Al	3.37	0.634	24
	3.29	0.62	13
	3.32	0.64	25
^{23}Na	2.62	0.25	24
	2.58	0.25	13

The sample of low albite used for the experiments in this paper came from Cazadero, CA. Several sets of quadrupolar parameters for low albite have been published in the literature[13,24,25] and are summarized in Table 2. The values of Kirkpatrick et al.[13] are used for all simulations in this paper. With quadrupolar frequencies of this magnitude and with ω_{1S} restricted to relatively low values due to the large coil size[26] used in some of the experiments (see section 3), spin locking in our cross-polarization experiments is limited to the sudden regime even at slow spinning speeds. In all simulations and measurements presented in this paper, α is less than 0.02.

To analyze the detailed behavior of the aluminum spin-lock efficiency at slow spinning speeds and low-rf fields, experiments were performed on a home-built spectrometer incorporating a Tecmag acquisition system operating at a proton Larmor frequency of 301.2 MHz, which corresponds to a ^{27}Al Larmor frequency of 78.5 MHz. A Chemagnetics MAS probe with a 4 mm pencil rotor was used, and spinning speeds were regulated to within $\pm$5 Hz by a home-built spinning speed controller. For each of the one-dimensional experiments 64 scans were summed with a recycle time of 5 s. The MAS spinning speed was 4000 Hz, and the selective 90° pulse length on the aluminum central transition was 17 μs, which corresponds to an rf field strength of $\omega_{1S}/(2\pi) = 4900$ Hz.

Spectra using eight different spin-lock times ($\tau_{SL} = 10$ μs, 1 ms, 5 ms, 10 ms, 20 ms, 50 ms, 100 ms, and 200 ms) were recorded for each of 28 different rf field strengths in the range from $\omega_{1S}/(2\pi) = 440$ Hz to $\omega_{1S}/(2\pi) = 4400$ Hz. This corresponds to a range of the adiabaticity parameter from $\alpha = 5 \times 10^{-5}$ to $\alpha = 5 \times 10^{-3}$. The integral of the central transition of the Fourier-transformed spectrum was used as a measure of the spin-lock efficiency for the corresponding rf field strength. Figure 1a shows the spin-lock efficiency for spin-lock times (τ_{SL}) of 10 μs, 1 ms, and 10 ms. As expected, the intensity at

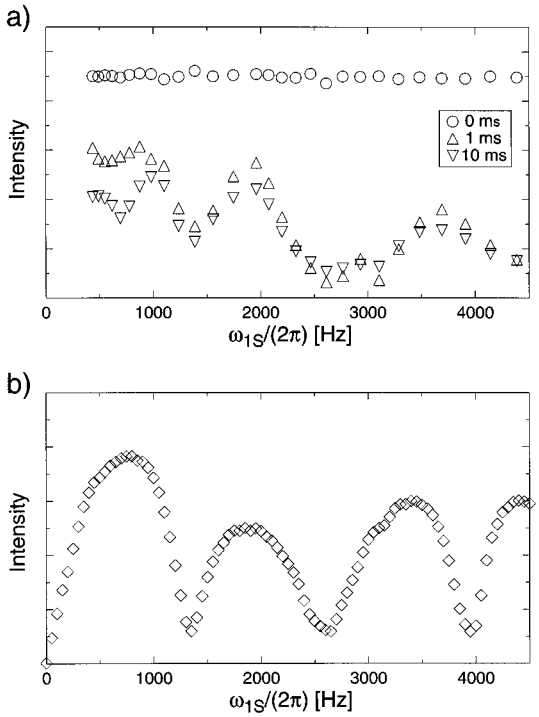

Figure 1. Spin-lock efficiency for ^{27}Al in albite during magic-angle spinning ($\omega_r/(2\pi) = 4000$ Hz) as a function of the rf field strengths. The ^{27}Al Larmor frequency is 78.5 MHz. (a) Integrated intensity of the aluminum central transition as a function of the rf field strength for experiments with spin-lock times (τ_{SL}) of 10 μs (○), 1 ms (△), and 10 ms (▽). (b) Simulations of the "equilibrium" spin-lock efficiency for a spin-$^5/_2$ nucleus including both first- and second-order quadrupolar interactions and using the parameters for aluminum in albite. Both measurements and simulations show distinct decays of spin-locked magnetization at one-third and two-thirds of the spinning speed.

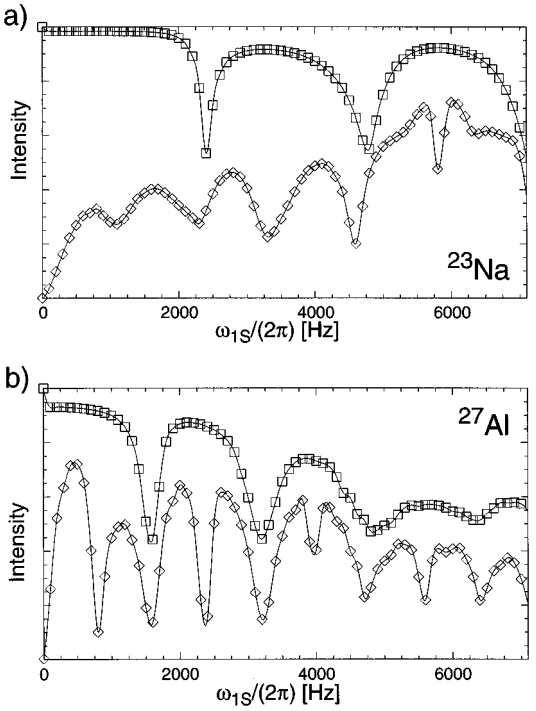

Figure 2. (a) Simulations of the spin-lock efficiency for ^{23}Na($S=^3/_2$) at an MAS frequency of $\omega_r/(2\pi) = 2400$ Hz both with [◇] and without [□] the second-order quadrupolar interaction. (b) Simulations of the spin-lock efficiency for ^{27}Al($S=^5/_2$) at an MAS frequency of $\omega_r/(2\pi) = 2400$ Hz both with [◇] and without [□] the second-order quadrupolar interaction. Solid lines are guides to the eye. For all simulations the quadrupolar parameters of low albite were used.[13]

$\tau_{SL} = 10$ μs is fairly constant and does not depend on the field strength. At longer spin-lock times, there is a very distinct dependence of the signal intensity on the rf field strength. In addition to rotating frame relaxation, there are dips at spin-lock field strengths approximately equal to one-third, two-thirds, and one times the rotor frequency. The measured intensities for spin-lock times of 1 and 10 ms are very similar, which indicates that the decay due to the time dependence of the quadrupolar interaction is very fast and occurs during the first few rotor cycles. The main differences between the spin-lock times of 1 and 10 ms occur at very low-rf field strengths and are most likely due to off-resonance effects.

The distinct dips in intensity found experimentally are clearly reflected in the numerical simulations shown in Figure 1b. These numerical simulations were performed using the NMR simulation package GAMMA.[27] To solve the Liouville−von Neumann equation for the time-dependent Hamiltonian, a small-step numerical integration with a time increment of 50 ns was performed. The simulations included the second-order quadrupolar Hamiltonian (eq 4) but omitted all relaxation effects. The Hilbert space was limited to a one-spin system; therefore, all scalar and dipolar couplings to other spins were neglected. The chemical shielding tensor and chemical shift offsets were also neglected in the simulations. A spinning speed of 4000 Hz and a ^{27}Al Larmor frequency of 78.5 MHz were used. Three hundred different crystallite orientations were averaged using the method of Cheng et al.[28] to approximate all crystallite orientations present in a powder sample. The simulated time domain data (intensity as a function of the spin-lock time) show a very rapid decay within the first 1 ms after which the intensity stabilizes and does not decay further due to the omission of relaxation effects from the numerical simulation. This equilibrium value is plotted as a function of the rf field strength in Figure 1b. The simulations show the same characteristic decays of the spin-lock efficiency for rf field strengths equal to one-third, two-thirds, and one times the rotor frequency as found in the experiment. At least some of the differences between the measurements and the simulations are due to the limitation of the simulation to a one-spin system. A similar level of agreement between experiment and simulation was found for other spinning speeds (data not shown).

A full theoretical analysis of the spin-lock behavior of quadrupolar nuclei under MAS is complicated by the fact that the Hamiltonian consists of a small time-independent term and a large time-dependent term. Consequently, analytical expressions for the interference process cannot be easily derived. We, therefore, performed numerical simulations to determine whether the interference effects between the mechanical sample rotation and the spin-lock field strength are due to the first-order or to the second-order terms of the quadrupolar Hamiltonian. Simulations of the spin-lock efficiency for ^{23}Na (spin $^3/_2$) and ^{27}Al (spin $^5/_2$) in low albite both with and without the second-order quadrupolar interaction were performed and are plotted as a function of the rf field strength in Figure 2. The MAS frequency was set to $\omega_r/(2\pi) = 2400$ Hz, which was the frequency used in the cross-polarization experiments of section 3, and 300 different crystallite orientations were averaged. The rf field strength was varied between $\omega_{1S}/(2\pi) = 0$ Hz and $\omega_{1S}/(2\pi) = 6800$ Hz for both the ^{23}Na and ^{27}Al nuclei. These parameters result in values of $\alpha < 0.019$ for ^{27}Al and $\alpha < 0.015$ for ^{23}Na, both well within the sudden-passage regime. The Larmor frequencies were 130.31 MHz for ^{27}Al and 132.28 MHz for ^{23}Na. The time increment for the numerical integration was 80 ns. There are clear differences in the positions of the resonance dips between the spin-$^3/_2$ and the spin-$^5/_2$ simulations,

but they follow a general rule. The spin-lock efficiency for simulations without the second-order quadrupolar interaction (denoted by □ in both parts of Figure 2) shows strong dips for the condition

$$\frac{\omega_{1S}}{\omega_r} = \frac{2N}{S + {}^1/_2} \tag{6}$$

where N is a positive integer and S is the spin quantum number of the spin-locked quadrupolar nucleus. At these dips, the efficiency decays to approximately 50% of the nonresonance value. The number of dips predicted by considering only the first-order quadrupolar interaction is, however, insufficient to characterize the experimentally observed spin-lock efficiency.

In the simulations which include the both the first- and second-order quadrupolar interactions (denoted by ◇ in Figures 1 and 2), the spin-lock efficiency decreases strongly when

$$\frac{\omega_{1S}}{\omega_r} = \frac{N}{S + {}^1/_2} \tag{7}$$

This leads to twice as many dips in the rf field dependence of the spin-lock efficiency as compared to the simulations without the second-order quadrupolar interaction and agrees with our experiments.

With increasing ω_Q, the overall efficiency of the spin lock decreases due to the large second-order quadrupolar Hamiltonian. This is the reason for the generally poorer spin-lock efficiency for the ^{23}Na in Figure 2a ($\omega_Q = 8.11 \times 10^6$ rad/s) as compared to the ^{27}Al in Figure 2b ($\omega_Q = 3.10 \times 10^6$ rad/s) for the simulations which include both first- and second-order terms. In making such comparisons, it is important to consider the values of ω_Q rather than the more commonly tabulated C_{qcc} values (see eq 3) since the $[2S(2S-1)]^{-1}$ scaling factor differs significantly for different values of S. In the case of low albite, for instance, the C_{qcc} for ^{23}Na($S={}^3/_2$) is less than the C_{qcc} for ^{27}Al($S={}^5/_2$), but the value of ω_Q for ^{23}Na is greater than the value of ω_Q for ^{27}Al. When smaller values of ω_Q are used in the simulations for ^{23}Na (data not shown), the resonances at low rf fields become sharper than in Figure 2a, and the spin-lock efficiency at points between the dips increases.

The simulations shown in Figure 2 were performed for the case of on-resonance irradiation. When rf offsets of several hundred hertz were incorporated into the simulations that only included the first-order contribution to the quadrupolar Hamiltonian, the spin-locking behavior became qualitatively similar to the second-order case, and eq 7 was obeyed.

Clearly, both first- and second-order terms of the quadrupolar Hamiltonian influence the spin-locking efficiency. However, it is important to consider the contributions of individual crystallite orientations to the powder average to determine whether the decreases in spin-lock efficiency are a property of the single-crystallite Hamiltonian itself or whether they are due to interference effects between different crystallite orientations. This has been partially discussed in the literature[20] and is examined here in more detail.

Figures 3 and 4 show spin-lock time dependences for a spin-$^5/_2$ nucleus (^{27}Al) with (f−j) and without (a−e) the second-order quadrupolar interaction for four different orientations (a−d and f−i) and for the powder average (e and j). For the simulations of Figure 3, the spinning speed was 2400 Hz, and the rf field strength was 800 Hz; these values satisfy the resonance condition of eq 7 but not that of eq 6. This is reflected in the fact that the simulations which exclude the second-order quadrupolar interaction (Figure 3a−e) show a good spin lock with only small-amplitude oscillations. Consequently the powder average (Figure 3e) shows almost no decay. Inclusion of the second-order quadrupolar interaction has a large effect on the spin-lock behavior (Figure 3f−j). The spin-locked magnetization oscillates between the positive and negative x axis at a frequency that depends strongly on the crystallite orientation. The interference between these different oscillation frequencies causes the fast decay observed in the powder (Figure 3j).

For the simulations of Figure 4, the resonance conditions of eqs 6 and 7 are simultaneously satisfied by setting the spinning speed equal to 2400 Hz and the rf field strength equal to 1600 Hz. In Figure 4 there are strong oscillations for both the simulations without (Figure 4a−e) and with (Figure 4f−j) the second-order quadrupolar interaction. However, when the second-order quadrupolar interaction is omitted, the oscillations are only between the positive maximum and zero (Figure 4a−d), leading to a reduced but nonvanishing value for the powder average (Figure 4e). Inclusion of the second-order interaction results again in oscillation between the positive maximum and its corresponding negative value (Figure 4f−i). Consequently, the powder average is almost zero (Figure 4j) due to the interference of magnetization from different crystallite orientations. Simulations for spin-lock fields in between resonance points (data not shown) show only small oscillations about nonzero values and thus good spin-lock efficiency. Similar calculations were performed for spin-$^3/_2$ nuclei and show the same general behavior as the spin-$^5/_2$ simulations discussed above.

The resonance conditions defined by eq 7 have an important consequence for cross-polarization experiments involving half-integer quadrupolar spins. Before setting up the cross-polarization condition, it is necessary to experimentally optimize the spin-lock efficiency of the quadrupolar nucleus for a given sample (i.e., given ω_Q) and spinning speed in order to avoid a severe loss of magnetization.

In addition to losses due to inefficient spin locking, the magnetization of quadrupolar nuclei under spin-lock conditions is further influenced by rotating-frame spin−lattice relaxation. Unlike for the case of spin-$^1/_2$ nuclei, the rotating-frame behavior of a quadrupolar nucleus cannot in general be modeled by a single exponential.[29,30] Consequently, no single relaxation time constant ($T_{1\rho}$) can be defined. In our experimental observations, rotating-frame relaxation of aluminum and sodium in albite consists of at least two exponentially decaying components. Figure 5 shows such a decay for ^{27}Al in albite for $\omega_{1S}/(2\pi) \approx$ 500 Hz and $\omega_r/(2\pi) = 2400$ Hz (the values used in the cross-polarization experiments of section 3). The solid curve in Figure 5 corresponds to a least-squares fit of the data to a biexponential function of the form

$$I(t) = A \exp\left(-\frac{t}{\tau_f}\right) + B \exp\left(-\frac{t}{\tau_s}\right) \tag{8}$$

in which the fast-decaying component is characterized by a time constant $\tau_f = 2.7$ ms, the slowly decaying component is characterized by a time constant $\tau_s = 85$ ms, and the scaling parameters have values of $A = 0.13$ and $B = 0.71$. The rotating-frame relaxation of ^{23}Na in albite also requires more than one exponential for a good fit. With typical cross-polarization contact times on the order of $\tau_{CP} = 10$ ms to $\tau_{CP} = 50$ ms, the rotating-frame relaxation of the quadrupolar nuclei in low albite poses no problems for efficient cross-polarization.

3. Cross-Polarization Dynamics

Using the results of the spin-lock efficiency study, we have investigated the ^{27}Al-to-^{29}Si cross-polarization dynamics in low

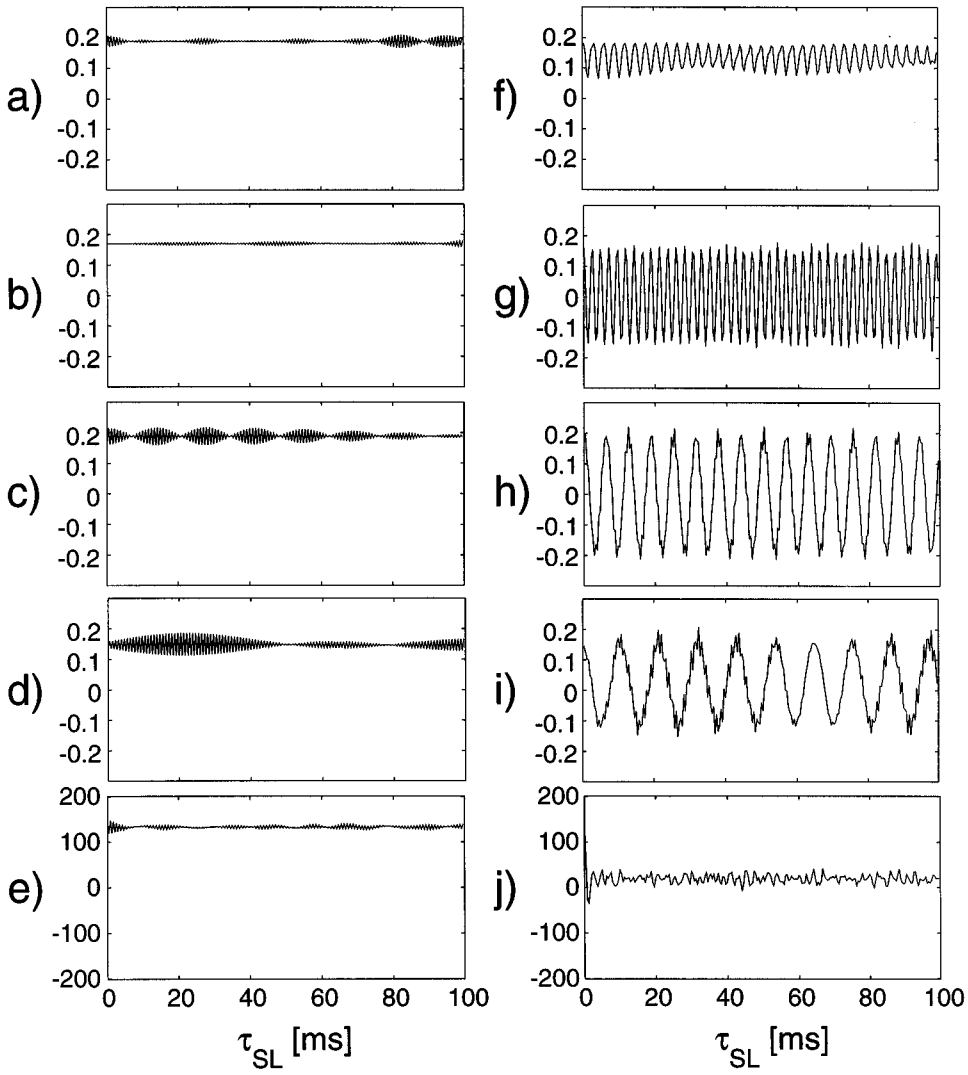

Figure 3. Simulated spin-lock efficiency for ^{27}Al at an MAS frequency of $\omega_r/(2\pi) = 2400$ Hz and a spin-lock field strength of $\omega_{1S}/(2\pi) = 800$ Hz. The Euler angles (α, β, γ) relate the principal-axis system of the quadrupolar interaction in a given crystallite to the reference frame of a rotor spinning at the magic angle. The simulations (a)−(e) were done without the second-order quadrupolar interaction while the simulations (f)−(j) include the second-order quadrupolar interaction. (a)−(d) and (f)−(i) show selected crystallite orientations with $\alpha = \gamma = 0°$ and $\beta = 10°$ ((a) and (f)), $\beta = 30°$ ((b) and (g)), $\beta = 50°$ ((c) and (h)), and $\beta = 70°$ ((d) and (i)). The simulations in (e) and (j) show the average over 1154 different crystallite orientations. For this choice of spinning speed and rf field strength, only the resonance condition of eq 7 is fulfilled. Therefore, the spin lock is very stable without the second-order quadrupolar interaction (e) but decays rapidly when the second-order quadrupolar interaction is included (j).

albite. Although cross-polarization was achieved from both ^{27}Al and ^{23}Na, we chose to concentrate on ^{27}Al since the cross-polarized signals were more intense. As mentioned in section 1, albite has three different silicon sites (see Table 1), two of which (Q^4(1Al)) have one aluminum atom and three silicon atoms as nearest neighbors while the third (Q^4(2Al)) has two aluminum atoms and two silicon atoms as nearest neighbors. On the basis of simple models, one might expect that the NMR signal intensity corresponding to the silicon with two aluminum atoms as nearest neighbors would be twice as intense as those of the silicons with only one aluminum atom as a nearest neighbor.[12] However, as a one-dimensional ^{29}Si NMR spectrum acquired using ^{27}Al-to-^{29}Si cross-polarization shows, this is not true in the case of low albite (Figure 6). The two silicon sites in albite with one aluminum nearest neighbor ($\delta = -96.1$ ppm and $\delta = -103.9$ ppm) have equal intensities while the site with two aluminum nearest neighbors ($\delta = -91.8$ ppm) has a lower intensity. There is no significant difference in the line widths of the three lines: the full width at half-maximum of a Lorentzian line fit was $\Delta\omega_{1/2} \approx 35$ Hz for all three lines. To investigate this behavior in more detail, we have performed cross-polarization contact-time dependence measurements as well as rotating-frame relaxation time measurements for the three silicon sites.

All cross-polarization experiments were performed on a Chemagnetics CMX-500 spectrometer operating at a proton Larmor frequency of 500.1 MHz. The ^{27}Al frequency was 130.31 MHz, the ^{23}Na frequency was 132.28 MHz, and the ^{29}Si frequency was 99.34 MHz. A home-built double-resonance MAS probe and a 14 mm pencil rotor supplied by Chemagnetics were used, and the spinning speed was controlled by a home-built spinning-speed controller to an accuracy of ±2 Hz. An MAS speed of 2400 Hz was used for all CP experiments and silicon $T_{1\rho}$ measurements described in this section. Typically, a 10−17 μs pulse was used for selective excitation of the central transition of aluminum. The cross-polarization was optimized experimentally based on the spin-lock efficiency for the central transition of the quadrupolar nucleus as a function of the rf field strength. At $\omega_r/(2\pi) = 2400$ Hz, the best spin-lock level for the ^{27}Al resonance was found to be $\omega_{1S}/(2\pi) \approx 500$ Hz, which agrees well with the simulations of Figure 2. The cross-polarization sequence used in these experiments incorporates

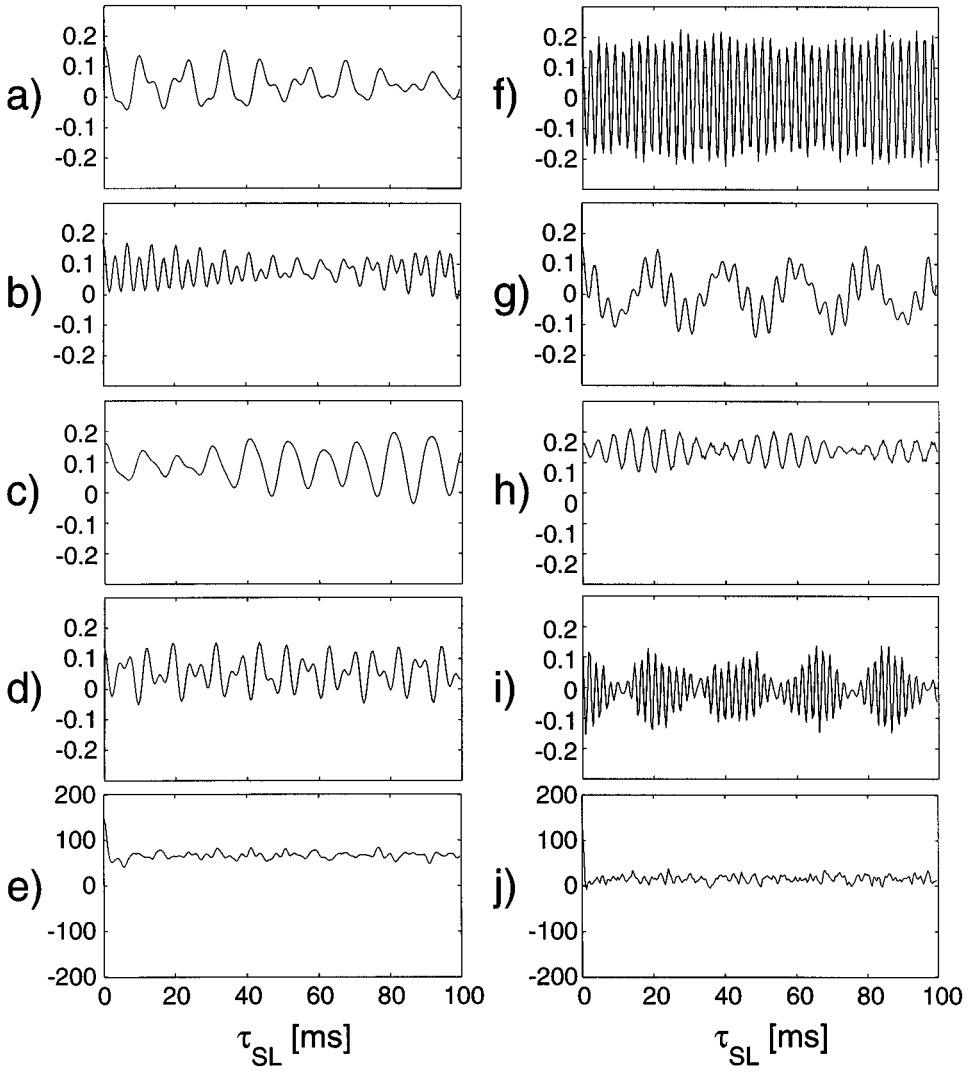

Figure 4. Simulated spin-lock efficiency for ^{27}Al at an MAS frequency of $\omega_r/(2\pi) = 2400$ Hz and a spin-lock field strength of $\omega_{1S}/(2\pi) = 1600$ Hz. The Euler angles (α, β, γ) relate the principal-axis system of the quadrupolar interaction in a given crystallite to the reference frame of a rotor spinning at the magic angle. The simulations (a)−(e) were done without the second-order quadrupolar interaction while the simulations (f)−(j) include the second-order quadrupolar interaction. (a)−(d) and (f)−(i) show selected crystallite orientations with $\alpha = \gamma = 0°$ and $\beta = 10°$ ((a) and (f)), $\beta = 30°$ ((b) and (g)), $\beta = 50°$ ((c) and (h)), and $\beta = 70°$ ((d) and (i)). The simulations in (e) and (j) show the average over 1154 different crystallite orientations. For this choice of spinning speed and rf field strength, the resonance conditions of eqs 6 and 7 are both fulfilled. Therefore, we see a fast decay of the spin-locked magnetization with (j) and without (e) the second-order quadrupolar interaction.

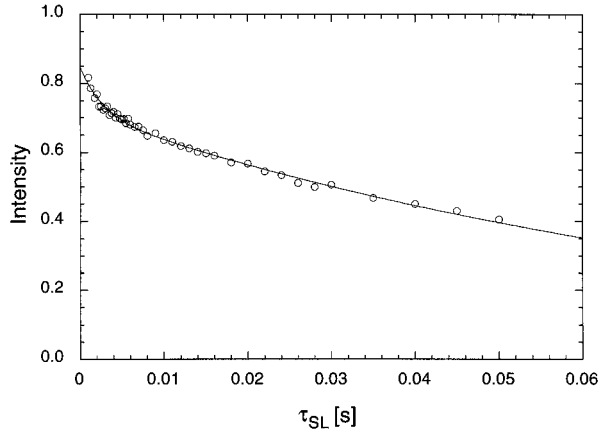

Figure 5. Rotating-frame relaxation of ^{27}Al in albite at $\omega_{1S}/(2\pi) \approx 500$ Hz and $\omega_r/(2\pi) = 2400$ Hz. The solid line is a nonlinear least-squares fit of the experimental points to a biexponential function with time constants of 2.7 and 85 ms.

spin-temperature alternation.[31] For the contact-time dependence study, cross-polarization signal intensities were measured for contact times (τ_{CP}) between 0.5 and 500 ms. For these measurements, 128 scans of 1024 data points were summed with a recycle delay of 5 s. Sixteen dummy scans preceded the collection of data. The silicon rotating-frame relaxation times ($T_{1\rho}$) were measured using the same parameters as for the CP time dependence studies but adding a spin-lock period after the CP contact time. On-resonance measurements were made for each site in both the CP dynamics and silicon $T_{1\rho}$ experiments to eliminate offset effects that are expected to occur at such low-rf power levels.

According to Hartmann and Hahn,[3] transfer of polarization between two different types of nuclei in a static sample can occur if the rf amplitudes are matched according to the condition

$$\sqrt{I(I+1) - m_I(m_I - 1)}\,\omega_{1I} = \sqrt{S(S+1) - m_S(m_S - 1)}\,\omega_{1S} \quad (9)$$

where $\omega_{1I} = |\gamma_{1I}B_{1I}|$, $\omega_{1S} = |\gamma_{1S}B_{1S}|$, I and S are spin quantum numbers, and the transitions being matched are between quantum levels $m \leftrightarrow (m - 1)$ for each nucleus. When polarization is transferred between a spin-$^1/_2$ nucleus (I) and

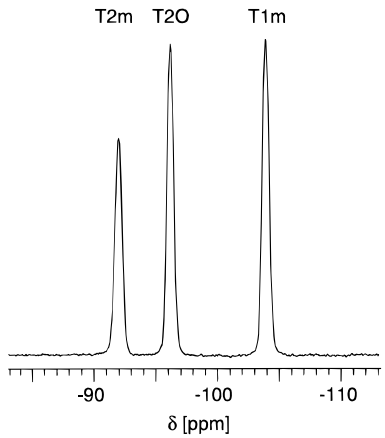

Figure 6. One-dimensional ^{29}Si spectrum of low albite obtained with cross-polarization from ^{27}Al. The crystallographic sites are indicated at the three different peaks. The peak at $\delta = -91.8$ ppm shows the lowest intensity although this silicon site has two nearest-neighbor aluminum atoms. The other two lines at $\delta = -96.1$ ppm and $\delta = -103.9$ ppm have roughly the same intensity.

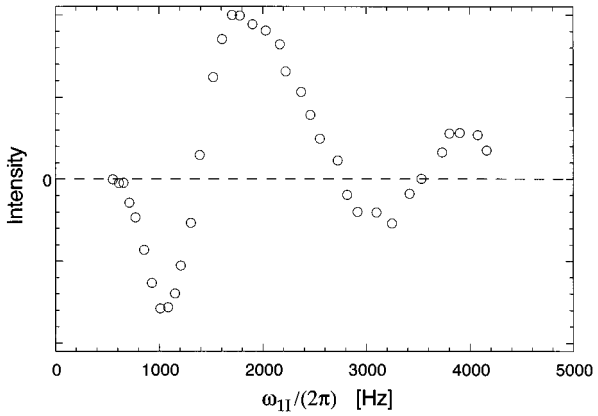

Figure 7. Intensity of signal cross-polarized from ^{27}Al to ^{29}Si as a function of ^{29}Si spin-lock field strength, $\omega_{1I}/(2\pi)$. The aluminum spin-lock field strength was $\omega_{1S}/(2\pi) \approx 500$ Hz, the spinning speed was $\omega_r/(2\pi) = 2400$ Hz, and a 50 ms contact time was used. The match condition clearly splits into sidebands, which is expected since the spinning speed is faster than the size of the aluminum homonuclear dipolar couplings. Some of the sidebands are folded over and appear with negative intensity.

the central transition of a half-integer quadrupolar nucleus (S), eq 9 simplifies to

$$\omega_{1I} = (S + {}^1/_2)\omega_{1S} \tag{10}$$

where S is the spin quantum number of the quadrupolar nucleus.

The Hartmann−Hahn match condition of eq 9 is modified by magic-angle spinning. For the case of transfer between two spin-$^1/_2$ nuclei, it has been shown[32,33] that when the rate of rotation, ω_r, equals or exceeds the strength of the homonuclear dipolar couplings, ω_d, the match condition of eq 9 splits into distinct sidebands

$$\omega_{1I} = \omega_{1S} + n\omega_r \tag{11}$$

where n is an integer. At short contact times the most efficient polarization transfer often occurs for the sidebands with $n = \pm 1, \pm 2$, but at longer contact times equally efficient transfer occurs for the centerband.[33] An analogous modification of the static cross-polarization condition has been proposed for transfer between a spin-$^1/_2$ nucleus and the central transition of a half-integer quadrupolar nucleus under MAS[7]

$$\omega_{1I} = (S + {}^1/_2)\omega_{1S} + n\omega_r \tag{12}$$

and has been observed experimentally.[12] Compared to the aluminum homonuclear dipolar couplings in low albite ($\omega_d/(2\pi) \approx 200$ Hz), we are in the "fast" spinning limit. Therefore, we expect to see the match condition split into sidebands under our experimental conditions.

Figure 7 shows the intensity of the signal cross-polarized from ^{27}Al to ^{29}Si in low albite as a function of the magnitude of the ^{29}Si rf field strength, $\omega_{1I}/(2\pi)$, for a cross-polarization contact time of $\tau_{CP} = 50$ ms. In these experiments the aluminum field strength was $\omega_{1S}/(2\pi) \approx 500$ Hz, and the spinning speed was $\omega_r/(2\pi) = 2400$ Hz. The centerband is at $\omega_{1I}/(2\pi) = 1500$ Hz, and the first positive ($n = +1$) sideband is at $\omega_{1I}/(2\pi) = 3900$ Hz. The $n = -1$ and $n = -2$ sidebands would be expected at negative field strengths and are therefore folded back with negative intensity.[33] Based on the parameters of the experiment, they should appear at $\omega_{1I}/(2\pi) \approx 900$ Hz and $\omega_{1I}/(2\pi) \approx 3300$ Hz. This agrees well with the experimental match condition of Figure 7; however, the precise positions of the centerband and sidebands are difficult to determine due to both the partial overlap of positive and negative sidebands and the difficulty of measuring low field strengths accurately. Higher order sidebands were also observed (data not shown), and the relative intensities of all sidebands remained nearly constant for contact times ranging between 10 and 750 ms.

The interference between different sideband matching conditions as seen in Figure 7 illustrates a second important consideration in setting up cross-polarization experiments involving half-integer quadrupolar nuclei at low-rf powers. In addition to optimizing the quadrupolar spin-lock efficiency for a given spinning speed (as described in section 2), one must make sure that the chosen spin-lock field strength and spinning speed create at least some sidebands of the match condition that do not interfere profoundly with other sidebands. Although the criteria for selecting efficient quadrupolar spin-lock field strengths eliminate some of the cases with the most destructive interference, there are other values of ω_{1S} and ω_r which give a good spin lock for the quadrupolar nucleus but for which the interference between the cross-polarization match sidebands would be severe. Furthermore, ω_r must be kept very stable since any change in the spinning speed will shift the positions of the folded-back sidebands and thereby alter the intensity of the cross-polarized signal. In our experimental setup we observed a change in the cross-polarized signal intensity of ~10% for a change in the spinning speed of 10 Hz. For both the CP contact-time dependence experiments and the silicon $T_{1\rho}$ measurements, we used the centerband match condition, which has relatively little overlap with the folded sidebands for our values of ω_{1S} and ω_r as Figure 7 shows.

In order to analyze the CP contact time dependence of the ^{29}Si magnetization, the rotating-frame relaxation rate constants for all three silicon sites were measured on-resonance at the rf field strength used for the cross-polarization experiments. Eight different time points from $\tau_{SL} = 500$ ms to $\tau_{SL} = 6$ s were measured four times each and fitted to a monoexponential decay. The relaxation times that were obtained are $T_{1\rho}(\delta = -91.8$ ppm$) = 5.8 \pm 0.2$ s, $T_{1\rho}(\delta = -96.1$ ppm$) = 12.8 \pm 1.1$ s, and $T_{1\rho}(\delta = -103.9$ ppm$) = 11.5 \pm 0.7$ s. It is interesting to see that the silicon site with two aluminum nearest neighbors has a $T_{1\rho}$ of only one-half the value of that for the silicon sites with only one aluminum nearest neighbor. The proportionality between the rate constant and the number of nearest neighbors suggests that the main relaxation pathway involves the aluminum atoms.

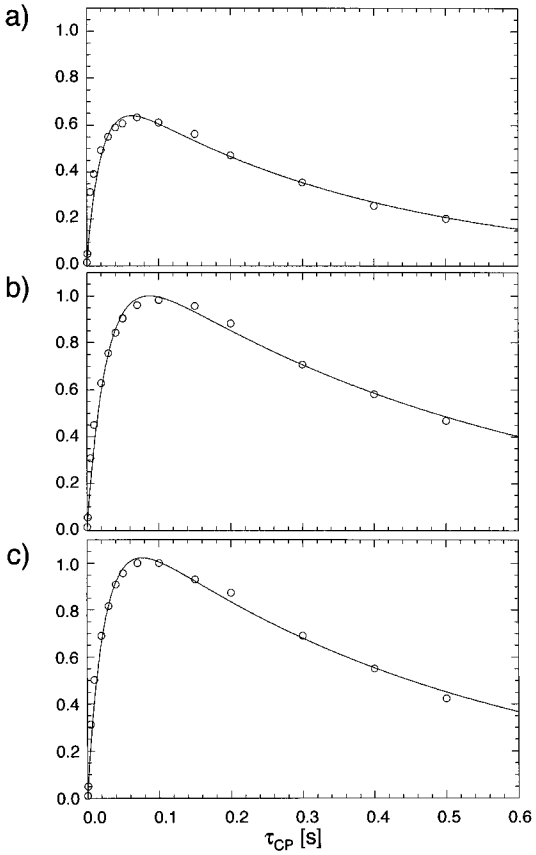

Figure 8. Cross-polarization time dependences for the three different crystallographic silicon sites in low albite: (a) the time dependence for the silicon $Q^4(2Al)$ site at $\delta = -91.8$ ppm; (b, c) the time dependences for the silicon $Q^4(1Al)$ sites at $\delta = -96.1$ ppm and $\delta = -103.9$ ppm, respectively. The fits through the experimental data points assume an analytical model (see eqs 13−15) based on a thermodynamic theory for spin-$^1/_2$ nuclei. The parameters extracted from these fits are summarized in Table 3.

Figure 8 shows the cross-polarization intensity as a function of contact time for all three silicon sites. The measurements were done as three separate on-resonance measurements to avoid resonance offset effects due to the low spin-lock field strengths. The most remarkable feature of these measurements is that the maximum polarization reached for the site with two aluminum nearest neighbors is lower than the maximum intensities of the two silicon sites with one aluminum nearest neighbor. The contact time dependences were fit to a simple model based on a thermodynamic description of cross-polarization.[34] This model makes no assumptions about whether the mechanism for magnetization transfer is based on the dipolar coupling interaction, the scalar coupling interaction, or both. The modifications necessary to describe cross-polarization involving the central transition of a half-integer quadrupolar nucleus[35] were included and lead to the following equation for the intensity of the I spin as a function of contact time:

$$I(\tau_{CP}) = \frac{S_0 \xi k_{SI}}{W}[\exp(-(k_S + k_I + k_{SI}(1+\lambda) + W)\tau_{CP}/2) - \exp(-(k_S + k_I + k_{SI}(1+\lambda) - W)\tau_{CP}/2)] \quad (13)$$

where

$$W = \sqrt{(k_S - k_I - k_{SI}(1-\lambda))^2 + 4{k_{SI}}^2\lambda} \quad (14)$$

S_0 is the initial S spin magnetization, k_I and k_S are the relaxation rate constants of the I and S spins, respectively, k_{SI} is the cross-polarization rate constant, and

$$\lambda = \frac{N_I\,(S + {}^1/_2)}{N_S\,(I + {}^1/_2)} \quad (15)$$

is a scaling factor describing the different spin environments. For the silicon sites with one aluminum nearest neighbor, λ is equal to 3 while for the silicon site with two aluminum nearest neighbors, λ equals $^3/_2$. Although most of the intensity in the ^{29}Si MAS spectrum of low albite at $\omega_r/(2\pi) = 2400$ Hz is concentrated in the centerbands, a few low-intensity sidebands are present for each site. Thus, a small correction factor, ξ, is included for each site so that the centerband intensities can be directly compared. ξ represents the fraction of the total intensity of a given site that is in the centerband. Because the principal values of the ^{29}Si chemical shielding tensors in low albite are known,[36] ξ can be calculated. At $\omega_r/(2\pi) = 2400$ Hz, ξ is equal to 0.76, 0.83, and 0.81 for the $\delta = -91.8$ ppm, $\delta = -96.1$ ppm, and $\delta = -103.9$ ppm sites, respectively. These values are quite similar to each other and show that, for our case, this is indeed a small correction. However, for slowly spun samples that contain sites with vastly different chemical shift anisotropies, the differences in ξ would be significant.

TABLE 3: Parameters for Cross-Polarization Time Dependence Fits

isotropic shift (ppm)	$k_I = 1/T_{1\rho}^{(I)a}$ (s^{-1})	$k_S = 1/T_{1\rho}^{(S)}$ (s^{-1})	$k_{SI} = 1/T_{CP}$ (s^{-1})	S_0
−91.8	0.17	45	2.8	17
−96.1	0.08	29	2.2	22
−103.9	0.09	33	2.4	25

[a] $T_{1\rho}^{(I)}$'s for silicon were measured by independent experiments and used as fixed parameters.

To determine the cross-polarization time dependences, the measured values of the silicon rotating-frame relaxation times ($k_I = 1/T_{1\rho}^{(I)}$) were used, and three-parameter fits were performed to extract values for S_0, k_S, and k_{SI}. The results of the best fits are summarized in Table 3. The rate constants for the cross-polarization process are, as expected, all in the same range since the distances to the nearest-neighbor aluminum atoms are very similar (see Table 1). However, the initial S spin magnetizations and the aluminum relaxation rate constants show a rather large and unexpected variation. Since there is only one aluminum site, one would expect to obtain very similar values for these two parameters.

To determine how sensitive such fits are to the parameters, eq 13 was used to generate simulated curves for several sets of parameters. Specifically, pairs of curves with identical values of S_0 and k_S were generated for $\lambda = {}^3/_2$ (the $Q^4(2Al)$ site) and for $\lambda = 3$ (the $Q^4(1Al)$ sites). The other parameters were varied but were constrained to have the same order of magnitude as the values in Table 3. The maxima of these simulated curves appeared especially sensitive to the value of k_{SI}. With just slight variations in the value of k_{SI}, the relative intensities of the $Q^4(2Al)$ and the $Q^4(1Al)$ sites changed considerably. In most cases, they were within a few percent of each other, but sometimes the $Q^4(2Al)$ site was more intense than the $Q^4(1Al)$ site and other times the converse was true. Thus, there is no simple relationship between the maximum intensity of the cross-polarized signal and the number of nearest-neighbor aluminum atoms for the conditions of our experiments. In view of these simulations, our experimental observation that the maximum intensity reached for the site with two aluminum nearest neighbors is lower than the maximum intensities of the two silicon sites with one aluminum nearest neighbor is not

TABLE 4: Principal Values[a] of ^{29}Si Chemical Shielding Tensors in Low Albite and Low Microcline

mineral	σ_{iso} (ppm)	σ_{11} (ppm)	σ_{22} (ppm)	σ_{33} (ppm)	η	$\Delta\sigma_{aniso}$ (ppm)
low albite	−91.8	−64 ± 4	−90 ± 3	−122 ± 5	0.9 ± 0.2	−30 ± 5
	−96.1	−74 ± 2	−93 ± 1	−121 ± 2	0.8 ± 0.1	−25 ± 2
	−103.9	−82 ± 2	−99 ± 2	−131 ± 2	0.6 ± 0.1	−27 ± 2
low microcline	−94.0	−58 ± 6	−94 ± 4	−130 ± 4	1.0 ± 0.2	−36 ± 6
	−96.4	−78 ± 2[b]	−94 ± 1[b]	−118 ± 1[b]	0.7 ± 0.1[b]	−21 ± 2[b]
	−99.5	−86 ± 4	−93 ± 2	−120 ± 3	0.3 ± 0.1	−20 ± 4

[a] The principal components of the chemical-shielding tensor are defined according to the convention of de Groot et al.[49] and were extracted by fitting the spinning sideband profile[49,50] of the anisotropic dimension for each site. [b] Since our sample of low microcline, like almost all samples found in nature,[42] contains domains of nearly pure albite, the peak at −96.4 ppm is actually due an overlap of albite and microcline resonances.

surprising and agrees qualitatively with the phenomenological theory. In fact, precise quantitative agreement between our data and eq 13 is not expected. The spin-temperature model we have used assumes an exponential decay of the spin-locked magnetization, but as pointed out in section 2, the relaxation of ^{27}Al in low albite is at least biexponential. The fact that there is no simple way to incorporate biexponential relaxation processes is one of the limitations of the phenomenological model. However, eq 13 is still a useful approximation. The values of $T_{1\rho}^{(S)}$ extracted from the fits (see Table 3) all fall into the physically reasonable range of being larger than the fast-decaying component and smaller than the slow-decaying component of the measured rotating-frame relaxation of ^{27}Al in low albite (see Figure 5).

Cross-polarization intensities often cannot be quantitatively interpreted even for the relatively simple case of cross-polarization between two spin-$^1/_2$ nuclei. When quadrupolar nuclei are involved, there is the additional complication that a selective pulse on the central transition will not uniformly excite all possible crystallite orientations. Thus, the value of λ for the Q^4(2Al) site would be expected to deviate from $^3/_2$. It is conceivable to correct for all these unknown scaling factors by explicitly taking the experimental conditions into consideration and simulating the relevant part of the spin system numerically. Such an approach may enable quantitative extraction of relative intensities from cross-polarization spectra involving half-integer quadrupolar nuclei.

4. Conclusions

In general, the improvement in signal-to-noise ratio that can be obtained by using cross-polarization depends on two factors: (1) the gyromagnetic ratio of the two spins and (2) their longitudinal relaxation times. The relaxation time determines how fast an experiment can be repeated, and a shorter relaxation time has the advantage of permitting faster signal averaging. In low albite, the signal-to-noise ratio per unit time was enhanced by a factor of 5 for the ^{27}Al-to-^{29}Si cross-polarization experiment relative to the direct excitation experiment when both were optimized. Performing the cross-polarization experiments with a linear amplitude ramp[37−39] on the spin-$^1/_2$ nuclei during the spin lock (data not shown) led to an additional 40% signal enhancement and a slight modification of the cross-polarization parameters. However, the relative heights of the three peaks did not change. Although in a single scan the signal obtained by cross-polarization is actually less intense than the direct excitation signal, there is a still a gain in the signal-to-noise ratio per unit time due to the faster repetition rate in the cross-polarization spectrum (5 s) compared to the direct excitation spectrum (2000 s).

The cross-polarization experiment gives less signal per scan than the direct excitation experiment because the cross-polarization efficiency for quadrupolar nuclei is usually very low for a sample spun about an angle greater than 30° from the static field due to the time dependence of the first-order quadrupolar interaction.[19,23] Although switched-angle spinning experiments take advantage of the increased cross-polarization efficiency for samples spun about an axis parallel to the static magnetic field,[10,19] they cannot be performed on conventional MAS equipment. Furthermore, the design of switched-angle spinning probes which are capable of spinning about an axis parallel to the static field[40,41] precludes the use of a large volume rotor, but use of a large rotor greatly enhances sensitivity. Thus, despite the loss in intensity per scan, cross-polarization from quadrupolar nuclei during MAS can still be a useful technique in many cases.

In addition to large differences in T_1 times, two other conditions must be fulfilled for cross-polarization from quadrupolar nuclei to be advantageous: (1) the quadrupolar coupling constant must be small enough to allow efficient spin locking, and (2) the $T_{1\rho}$ relaxation times of both spins must be long compared to the inverse of the cross-relaxation rate constant.

Optimization of polarization transfer from the quadrupolar nucleus is more difficult than in the spin-$^1/_2$ case because of interference effects between the spin-lock field strength and the spinning speed. The spin-lock efficiency at low-rf field strengths and slow spinning speeds shows characteristic resonant decays if the rf field strength is an integer multiple of the spinning speed divided by the sum of the spin quantum number and one-half. The location and number of the resonance conditions depend on whether the contributions from the second-order quadrupolar interaction or the offset are significant. Based on the choice of the rf field strength for the quadrupolar nucleus, the Hartmann−Hahn match must then also be experimentally optimized. It is important to avoid destructive overlap of the centerband and folded sidebands from the Hartmann−Hahn match.

The cross-polarization time dependences clearly show that one should not expect a direct correlation between the peak intensity and the number of nearest-neighbor atoms in all cases. There is a qualitative agreement with the theoretical predictions of a thermodynamical model, but there are differences in the quantitative behavior. If a quantitative evaluation of intensities is required, numerical simulations of the relevant spin systems and the experimental conditions could be used to obtain the relative scaling factors, which would then allow the extraction of information about the environments of the various sites.

An advantage of the faster repetition rate for ^{27}Al-to-^{29}Si cross-polarization is the increased feasibility of two-dimensional experiments since a 5-fold increase in signal enhancement corresponds to a 25-fold savings in time. We have used cross-polarization from ^{27}Al-to-^{29}Si to measure two-dimensional ^{29}Si isotropic−anisotropic correlation spectra using several different pulse sequences, all of which require only standard MAS equipment. Table 4 shows the measured principal values of the ^{29}Si chemical shielding tensors for different sites in low albite and low microcline. Due to the presence of domains of low albite in almost all samples of low microcline,[42] the one-dimensional ^{29}Si MAS NMR spectrum of low microcline has

many overlapping peaks, and the principal values of the chemical shift tensors could not have been determined from a one-dimensional spectrum. A detailed discussion of the methods for measuring such chemical shielding tensors will be published elsewhere.[36]

Another example of a use for cross-polarization from quadrupolar nuclei during MAS is in heteronuclear correlation experiments[43−45] designed to extract qualitative information about connectivities between atoms. Such experiments have been performed for quadrupolar nuclei under MAS conditions.[8,9,12,46−48] However, care must be taken in the choice of the spinning speed and the rf field as described in section 2. If these parameters are not set carefully, destructive interference between the spinning speed and the spin-lock field strength would give the same result (no cross peak) as a lack of connectivity between sites.

Acknowledgment. This work was supported by the Director, Office of Energy Research, Office of Basic Energy Sciences, Materials Sciences Division, U.S. Department of Energy, under Contract DE-AC03-76SF00098. Research support from Otsuka Electronics/Chemagnetics is also acknowledged. The authors thank Dr. H. J. M. de Groot for providing a sideband simulation program. S.M.D. thanks the National Science Foundation for a graduate fellowship. M.E. thanks the Deutsche Forschungsgemeinschaft for a postdoctoral fellowship (Grant Er 214/1-1).

References and Notes

(1) Fyfe, C. A. *Solid State NMR for Chemists*; C.F.C. Press: Guelph, 1983.
(2) Engelhardt, G.; Koller, H. In *Solid State NMR II: Inorganic Matter*; Blümich, B., Ed.; Springer-Verlag: Berlin, 1994; Vol. 31.
(3) Hartmann, S. R.; Hahn, E. L. *Phys. Rev.* **1962**, *128*, 2042.
(4) Pines, A.; Gibby, M. G.; Waugh, J. S. *J. Chem. Phys.* **1973**, *59*, 569.
(5) Schaefer, J.; Stejskal, E. O. *J. Am. Chem. Soc.* **1976**, *98*, 1031.
(6) Vega, A. J. *J. Magn. Reson.* **1992**, *96*, 50.
(7) Vega, A. J. *Solid State NMR* **1992**, *1*, 17.
(8) Fyfe, C. A.; Grondey, H.; Mueller, K. T.; Wong-Moon, K. C.; Markus, T. *J. Am. Chem. Soc.* **1992**, *114*, 5876.
(9) Fyfe, C. A.; Mueller, K. T.; Grondey, H.; Wong-Moon, K. C. *J. Phys. Chem.* **1993**, *97*, 13484.
(10) Fyfe, C. A.; Wong-Moon, K. C.; Grondey, H.; Mueller, K. T. *J. Phys. Chem.* **1994**, *98*, 2139.
(11) Kolodziejski, W.; Corma, A. *Solid State NMR* **1994**, *3*, 177.
(12) Fyfe, C. A.; Wong-Moon, K. C.; Huang, Y.; Grondey, H.; Mueller, K. T. *J. Phys. Chem.* **1995**, *99*, 8707.
(13) Kirkpatrick, R. J.; Kinsey, R. A.; Smith, K. A.; Henderson, D. M.; Oldfield, E. *Am. Mineral.* **1985**, *70*, 106.
(14) Harlow, G. E.; Brown, J. *Am. Mineral.* **1980**, *65*, 986.
(15) Smith, K. A.; Kirkpatrick, R. J.; Oldfield, E.; Henderson, D. M. *Am. Mineral.* **1983**, *68*, 1206.
(16) Woessner, D. E.; Trewella, J. C. *J. Magn. Reson.* **1984**, *59*, 352.
(17) Lippmaa, E.; Mägi, M.; Samoson, A.; Engelhardt, G.; Grimmer, A.-R. *J. Am. Chem. Soc.* **1980**, *102*, 4889.
(18) Smith, J. V.; Blackwell, C. S.; Hovis, G. L. *Nature* **1984**, *309*, 140.
(19) Baltisberger, J. H.; Gann, S. L.; Grandinetti, P. J.; Pines, A. *Mol. Phys.* **1994**, *81*, 1109.
(20) Sun, W.; Stephen, J. T.; Potter, L. D.; Wu, Y. *J. Magn. Reson., Ser. A* **1995**, *116*, 181.
(21) Haeberlen, U. *High Resolution NMR in Solids—Selective Averaging*; Academic Press: New York, 1976.
(22) Goldman, M.; Grandinetti, P. J.; Llor, A.; Olejniczak, Z.; Sachleben, J. R.; Zwanziger, J. W. *J. Chem. Phys.* **1992**, *97*, 8947.
(23) Baltisberger, J. H. Ph.D. Thesis, University of California, Berkeley, 1993.
(24) Brun, E.; Hafner, S.; Hartmann, P. *Helv. Phys. Acta* **1960**, *33*, 495.
(25) Woessner, D. E.; Timken, H. K. C. *J. Magn. Reson.* **1990**, *90*, 411.
(26) Fukushima, E.; Roeder, S. B. W. *Experimental Pulse NMR: A Nuts and Bolts Approach*; Addison-Wesley: Reading, MA, 1981.
(27) Smith, S. A.; Levante, T. O.; Meier, B. H.; Ernst, R. R. *J. Magn. Reson., Ser. A* **1994**, *106*, 75.
(28) Cheng, V. B.; Henry, H.; Suzukawa, J.; Wolfsberg, M. *J. Chem. Phys.* **1973**, *59*, 3992.
(29) Cohen, M. H.; Reif, F. In *Solid State Physics*; Seitz, F., Turnbull, D., Eds.; Academic Press: New York, 1957; Vol. 5.
(30) Seliger, J. *J. Magn. Reson., Ser. A* **1995**, *116*, 67.
(31) Stejskal, E. O.; Schaefer, J. *J. Magn. Reson.* **1975**, *18*, 560.
(32) Stejskal, E. O.; Schaefer, J.; Waugh, J. S. *J. Magn. Reson.* **1977**, *28*, 105.
(33) Meier, B. H. *Chem. Phys. Lett.* **1992**, *188*, 201.
(34) Mehring, M. *Principles of High-Resolution NMR in Solids*; Springer-Verlag: Berlin, Germany, 1976.
(35) Walter, T. H.; Turner, G. L.; Oldfield, E. *J. Magn. Reson.* **1988**, *76*, 106.
(36) Shore, J. S.; De Paul, S. M.; Ernst, M.; Stebbins, J. F.; Pines, A., to be published.
(37) Zhang, S. *J. Magn. Reson., Ser. A* **1994**, *110*, 73.
(38) Metz, G.; Wu, X.; Smith, S. O. *J. Magn. Reson., Ser. A* **1994**, *110*, 219.
(39) Zhang, S.; Czekaj, C. L.; Ford, W. T. *J. Magn. Reson., Ser. A* **1994**, *111*, 87.
(40) Mueller, K. T.; Chingas, G. C.; Pines, A. *Rev. Sci. Instrum.* **1991**, *62*, 1445.
(41) Tomaselli, M.; Meier, B. H.; Baldus, M.; Eisenegger, J.; Ernst, R. R. *Chem. Phys. Lett.* **1994**, *225*, 131.
(42) Smith, J. V. *Feldspar Minerals*; Springer-Verlag: Berlin, 1988.
(43) Caravatti, P.; Braunschweiler, L.; Ernst, R. R. *Chem. Phys. Lett.* **1983**, *100*, 305.
(44) Roberts, J. E.; Vega, S.; Griffin, R. G. *J. Am. Chem. Soc.* **1984**, *106*, 2506.
(45) Vega, A. J. *J. Am. Chem. Soc.* **1988**, *110*, 1049.
(46) Fyfe, C. A.; Mueller, K. T.; Grondey, H.; Wong-Moon, K. C. *Chem. Phys. Lett.* **1992**, *199*, 198.
(47) Almond, G. G.; Harris, R. K.; Franklin, K. R. *Solid State NMR* **1996**, *6*, 31.
(48) Wang, S. H.; De Paul, S. M.; Bull, L. M. *J. Magn. Reson.*, in press.
(49) de Groot, H. J. M.; Smith, S. O.; Kolbert, A. C.; Courtin, J. M. L.; Winkel, C.; Lugtenburg, J.; Herzfeld, J.; Griffin, R. G. *J. Magn. Reson.* **1991**, *91*, 30.
(50) Herzfeld, J.; Berger, A. E. *J. Chem. Phys.* **1980**, *73*, 6021.